eXPRESS
Polymer Letters

Synthesis and characterization of polypyrrole doped with anionic spherical polyelectrolyte brushes

N. Su[1], H. B. Li[1]*, S. J. Yuan[2], S. P. Yi[3], E .Q. Yin[1]

[1]School of Printing and Packaging, Wuhan University, 430079 Wuhan, China
[2]School of Chemical and Environmental Engineering, Hubei University of Technology, 430068 Wuhan, China
[3]College of Chemistry and Molecular Sciences, Wuhan University, 430072 Wuhan, China

Abstract. The procedures for the synthesis of polypyrrole (PPy) doped with anionic spherical polyelectrolyte brushes (ASPB) (PPy/ASPB nanocomposite) by means of *in situ* chemical oxidative polymerization were presented. Fourier transform infrared spectroscopy (FTIR) and Raman spectroscopic analysis suggested the bonding structure of PPy/ASPB nanocomposite. Scanning electron microscopy (SEM) was used to confirm the morphologies of samples. The crystallographic structure, chemical nature and thermal stability of conducting polymers were analyzed by X-ray diffraction (XRD), X-ray photoelectron spectroscopy (XPS) and Thermo-gravimetric analysis (TGA) respectively. Investigation of the electrical conductivity at room temperature showed that the electrical conductivity of PPy/ASPB nanocomposite was 20 S/cm, which was higher than that of PPy (3.6 S/cm).

Keywords: nanocomposites, conducting polymers, anionic spherical polyelectrolyte brushes, doping, electrical conductivity

1. Introduction

Since the first paper of Shirakawa *et al.* [1] in 1977, conducting polymers have attracted considerable interest because of their excellent physical and chemical properties originating from their unique π-conjugated system [2]. Polypyrrole (PPy) is one of the most extensively studied materials due to its easy synthesis and good environmental stability [3, 4]. However, pristine PPy is insoluble and infusible because of the rigidity of its molecular chains of π-conjugated structure. This poor conductivity and processibility not only impede further investigation of its structure, but also limit its application in technology. So efforts to overcome these drawbacks have led to numerous studies on the synthesis of PPy by both electrochemical and chemical routes.

It is well-known that using various dopants has contributed to the development of soluble PPy [5]. Currently, aromatic acid derivatives and organic sulfonates are widely used, such as dodecylbenzene sulfonic acid (DBSA), p-toluenesulfonic acid (TsOH) [6], etc. Lee *et al.* [7] developed DBSA with surface-active properties as anionic additive to realize pyrrole (Py) solvation. Further studies pointed out that adding other large dopants could reduce the interchain links, resulting in the increase of the conductivity and solubility [8–11]. In view of this, anionic spherical polyelectrolyte brushes (ASPB), consisting of anion polyelectrolyte chains affixing to the surface of spheres, may be novel conducting polymer dopant by introducing the brush polymer with certain functional groups.

The investigations on the structure and properties of PPy have been performed by many techniques. X-ray photoelectron spectroscopy (XPS) proved to be particularly useful in the surface characterization of

PPy [12–14] because it has a typical sampling depth of 2–10 nm. Fourier transform infrared spectroscopy (FTIR) is a convenient technique to monitor changes in the structure of conducting polymer chains [15, 16]. Both experimental methods [17] and theoretical model [18] have been developed to describe the dependence of conductivity on conjugation length for PPy from FTIR measurements. In addition, Raman spectra [6], X-ray diffraction (XRD) [19], and Thermo-gravimetric analysis (TGA) [20] are also used to study the structure and properties of PPy.

In this paper, we presented a facile method for the synthesis of PPy doped with ASPB (PPy/ASPB nanocomposite) by *in situ* chemical oxidative polymerization [21, 22]. For comparison, PPy was synthesized first. The morphology of the resulting PPy/ASPB nanocomposite was characterized by scanning electron microscopy (SEM). Information about its structure was obtained from FTIR, Raman spectra, XRD techniques, and its surface chemical composition by XPS measurements. The room temperature electrical conductivities and thermal stability of PPy and PPy/ASPB nanocomposite were investigated by a four-point probe apparatus and TGA respectively.

2. Experimental
2.1. Materials
Pyrrole (Sinopharm of Chemical Reagents Co., Ltd, Shanghai, China) was distilled under reduced pressure before use. Iron (III) chloride hexahydrate ($FeCl_3 \cdot 6H_2O$) and ethanol were purchased from Sinopharm of Chemical Reagents Co., Ltd, Shanghai, China. They were analytical reagents and were used without further purification. The ASPB ($D_z \approx 100$ nm, $M_w = 1800$ g/mol, $M_w/M_n = 1.6$) consisting of modified SiO_2 cores and poly(Sodium-p-Styrenesulfonate) (PSS) brushes were prepared by surface-initiated polymerization.

2.2. Synthesis of PPy/ASPB nanocomposite
The synthesis of PPy/ASPB nanocomposite mainly involved: 0.22 g of ASPB was firstly added into 45 mL mixture of water and ethanol (v/v, 2/1) with ultrasonic dispersion for 20 min followed by addition of 1.34 g of distilled Py (0.2 mol). After the mixture was cooled to 5°C and degassed under N_2

flow for 15 min, 2.7 g (0.1 mol) of $FeCl_3 \cdot 6H_2O$ in 15 mL water aqueous solution was added, and the reaction was allowed to continue for 6 h. The resulting products were then collected via filtration, and were subjected to three sequential washings with ethanol and distilled water before finally being dried in vacuum at 60°C for 12 h.

2.3. Characterization methods
2.3.1. Morphological and structural analysis
Morphological studies were carried out using a Quanta 200 (FEI Company, Netherlands) scanning electron microscope (SEM) operated at 30 kV. FTIR spectra for PPy and PPy/ASPB nanocomposite were obtained using a Nicolet AVATAR 360FT spectrometer (Thermo Nicolet Corporation, USA). Raman spectra were obtained with a RW-1000 system (Renishaw Company, London, United Kingdom) using a Ar^+ laser operating at 514.5 nm with a CCD detector. X-Ray diffraction (XRD) measurements were carried out on a Shimadzu 'XRD-6000' instrument (Kyoto, Japan) operating at a voltage of 40 kV and a current of 40 mA with CuK_α radiation ($\lambda = 1.54060$ Å). The samples were measured in a continuous scan mode at 10–60° (2θ) with a scanning rate of 5°/min. XPS spectra were recorded using a VGESCALAB MK II system (United Kingdom) operated in the constant analyzer energy mode.

2.3.2. Electrical conductivity and thermal analysis
TGA was performed on a SETSYS-1750 instrument at a heating rate of 10°C/min in N_2 atmosphere. The electrical conductivities of the samples were measured in a four-point probe (RTS-4, China) apparatus at room temperature. After the samples were pressed into the circular tablet with $D = 13$ mm at 20 MPa, the thickness W of each tablet was measured. Then $F(W/S)$ and $F(D/S)$ ($S = 1$) were looked up from a table to calculate the source current I according to formula (1). $F(W/S)$ denoted the width correction coefficient, and $F(D/S)$ the diameter correction coefficient. Since conductivity (σ; S/cm) $= 1/\rho$, the electrical conductivities of resulting products could be calculated by Equation (1):

$$I = F(W/S) \cdot F(D/S) \cdot W \cdot 0.1 \tag{1}$$

3. Results and discussion

3.1. Morphologies

Figure 1 displays the morphologies of samples, and the schematic representations of formation mechanisms are shown in Figure 2. As shown by the SEM images, PPy displays a typically cauliflower-like or tumor-like structure (Figure 1a, b). The performance of three-dimensional (3D) polymer growth can be considered as quasi network systems through the 2, 3 coupling modes as shown in Figure 2a, supported by the 3D VRH (Variable range hopping) for $\sigma_{dc}(T)$ [23]. The interchain links or side chains through the 2, 3 coupling modes can lead to the poor solubility of PPy in organic solvents [24]. The addition of ASPB with uniform spherical structure (Figure 1d) provides the space factors for Py orderly growth (Figure 2b), resulting in special morphology of PPy. As shown in Figure 1c, PPy/ASPB nanocom-posite shows sphere-like structure and the particle size is much less than that of PPy (Figure 1a). Therefore, the SEM results elucidate that the reactions are remarkably effective for the PPy functionalization.

3.2. FTIR and Raman spectra studies

FTIR spectra of samples are represented in Figure 3. The FTIR spectrum of PPy shows the characteristic bands attributable to the C–H in-plane deformation vibration at 1039 cm^{-1}, C–C asymmetric stretching vibration at 1458 cm^{-1}, ring-stretching mode of Py ring at 1540 cm^{-1} [25]. These characteristic peaks from PPy are clearly shown in the FTIR spectrum of PPy/ASPB nanocomposite (1036, 1451 and 1546 cm^{-1}). In addition, PPy/ASPB nanocomposite shows some new bands: the broad band at 1292 cm^{-1} is attributed to C–H and C–N in-plane deformation
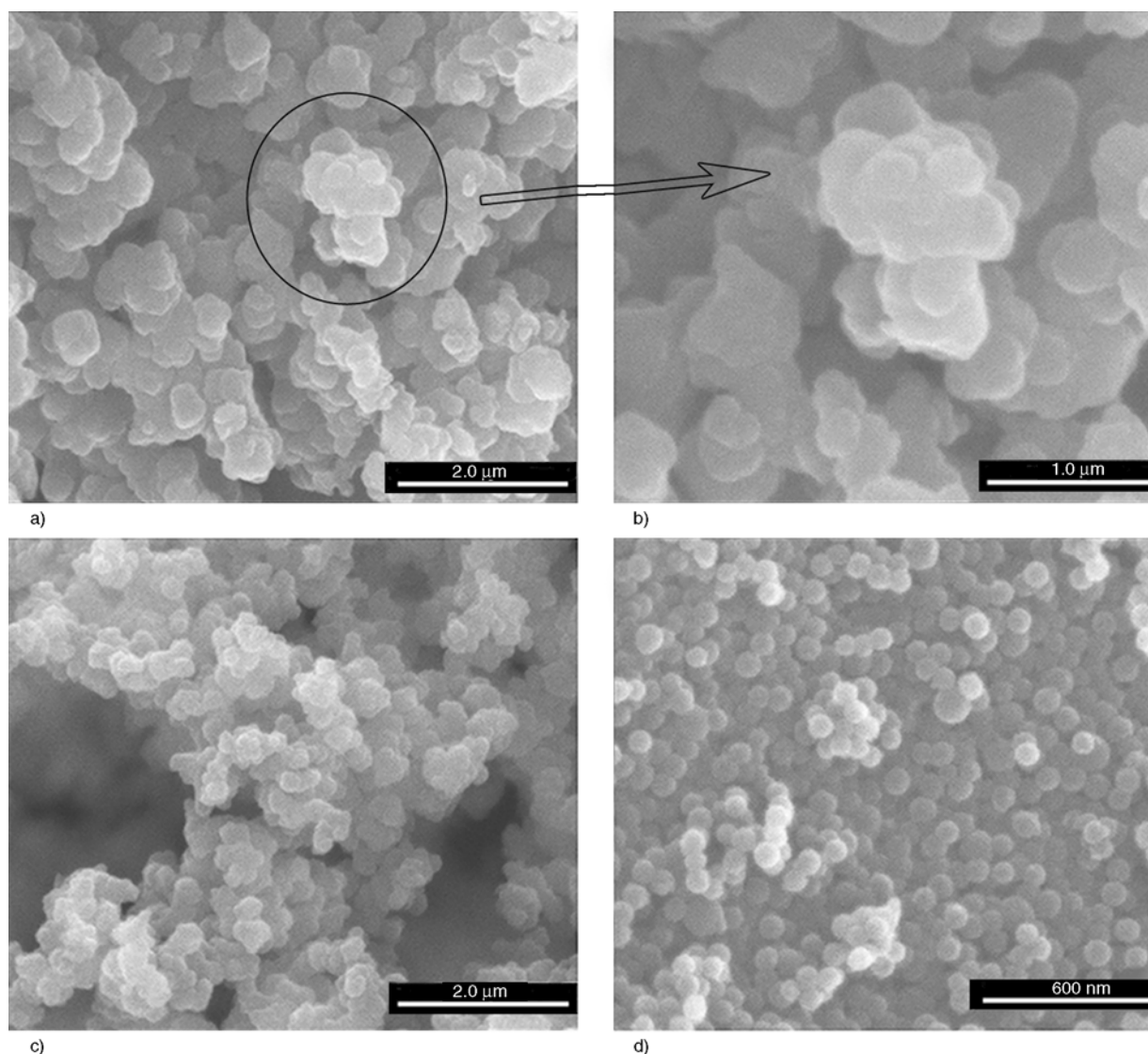

Figure 1. SEM images of PPy (a, b), PPy/ASPB nanocomposite (c) and ASPB (d)
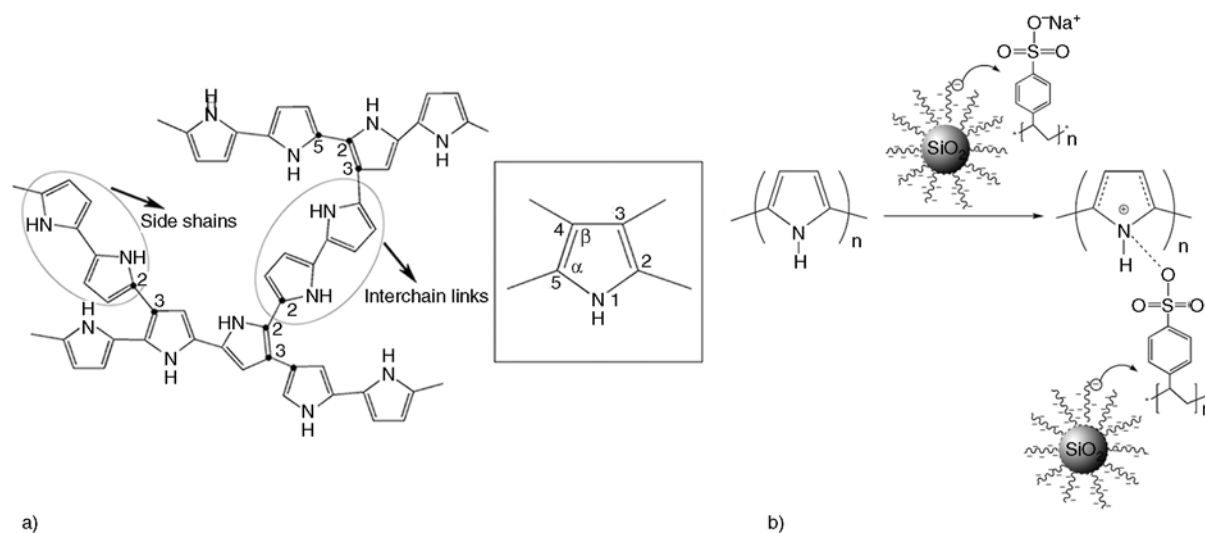
Figure 2. Schematic representations of formation mechanisms of PPy (a) and PPy/ASPB nanocomposite (b)
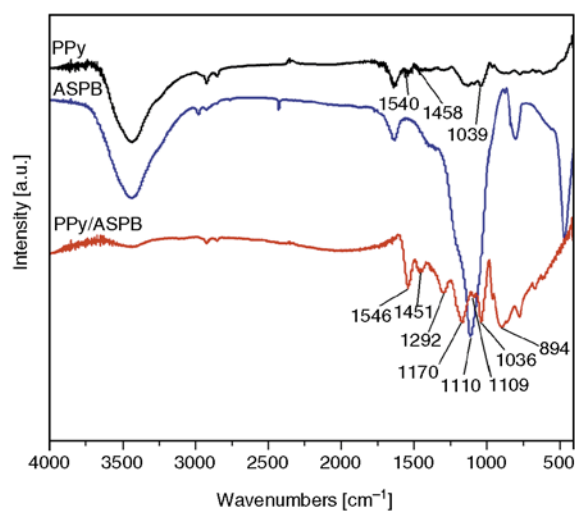

Figure 3. FTIR spectra of PPy, ASPB, and PPy/ASPB nanocomposite

Figure 4. Raman spectra of PPy and PPy/ASPB nanocomposite

vibrations; the strong bands at 1170 and 894 cm^{-1} are characteristic of doped PPy chains [11]. The peak at 1109 cm^{-1} may be attributed to Si–O–Si stretching vibrations, which appears at 1110 cm^{-1} in the spectrum of ASPB, suggesting that ASPB have already been doped in PPy system. In addition, the ratio of the integrated absorption areas of the 1451 and 1546 cm^{-1} (A_{1451}/A_{1546}) bands for the PPy/ASPB nanocomposite is 0.38, which is higher than that of PPy ($A_{1458}/A_{1540} = 0.27$). This suggests the conjugation length increases [17].

Figure 4 shows the Raman spectra of PPy and PPy/ASPB nanocomposite. The prominent bands that emerged in the spectrum of PPy can also be observed in the spectrum of PPy/ASPB nanocompos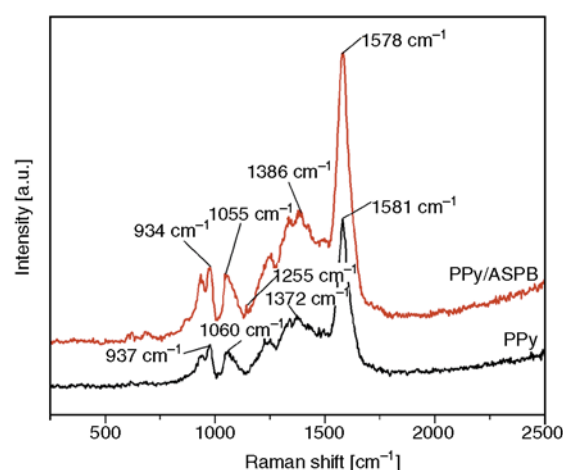ite. The appearance of peak at 1055 cm^{-1} (1060 cm^{-1} for PPy) has been associated with the quinonoid polaron structure and those at 934 cm^{-1} (937 cm^{-1} for PPy) and 1255 cm^{-1} (no presence in PPy spectrum) have been associated with the quinonoid bipolaron structure, revealing the presence of doped PPy structures [6, 26]. The peak at 1578 cm^{-1} (1581 cm^{-1} for PPy) attributable to C=C stretching is considered to be an overlap of two oxidized structures. Therefore, compared with the PPy, PPy/ASPB nanocomposite has an increased portion of bipolarons (1255 cm^{-1}) relative to polarons in the Raman spectrum, leading to the high conductivity [27].

3.3. Crystallographic structure

The crystallographic structures of samples are characterized using XRD measurements. As shown in Figure 5, PPy only exhibits a broad characteristic
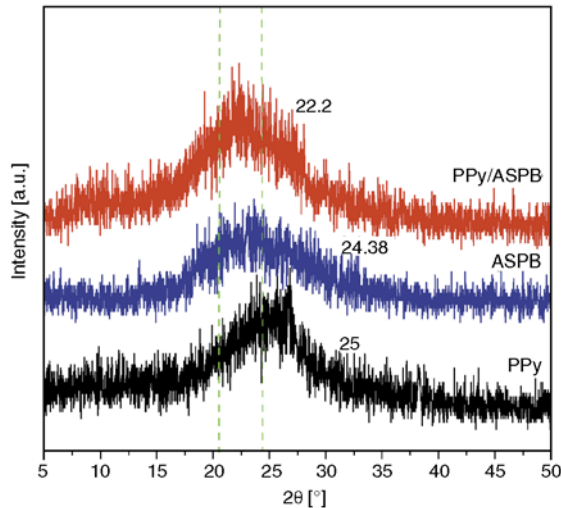
Figure 5. XRD patterns of PPy, ASPB and PPy/ASPB nanocomposite

peak at $2\theta = 25$ °, implying an amorphous structure [28]. For the XRD pattern of ASPB, the characteristic peak at $2\theta = 24.38°$ appears, corresponding to SiO_2 reflection peak. For the PPy/ASPB nanocomposite, the broad characteristic peak has shifted to 22.2°. The changes may be due to the doping of

ASPB (SiO_2 cores) into conducting polymer matrix. In addition, full width at half maximum (FWHM) of PPy/ASPB nanocomposite (10.1°) is higher than that of PPy (7.6°), which confirms that the crystallinity of PPy/ASPB nanocomposite is decreased, which helps to the increase of solubility.

3.4. XPS study

Wide region spectroscopy of PPy and PPy/ASPB nanocomposite are shown in Figure 6a. The narrow range spectra of C_{1s}, O_{1s} and N_{1s} of PPy/ASPB nanocomposite are also depicted (Figure 6b–6d). Compared with the wide region spectroscopy of PPy, the peaks at 101.9 and 167.3 eV for PPy/ASPB nanocomposite spectrum have been observed, suggesting the existence of Silicon and Sulfur signals respectively (from ASPB).

For the chemically synthesized PPy/ASPB nanocomposite, the C_{1s} main peak is decomposed into five lines (Figure 6b). The lowest binding energy centered peak (main C peak) at 284.1 eV corresponds to the β-carbons of Py ring and covalent bonded carbon in the ASPB dopant, while the binding energy cen-
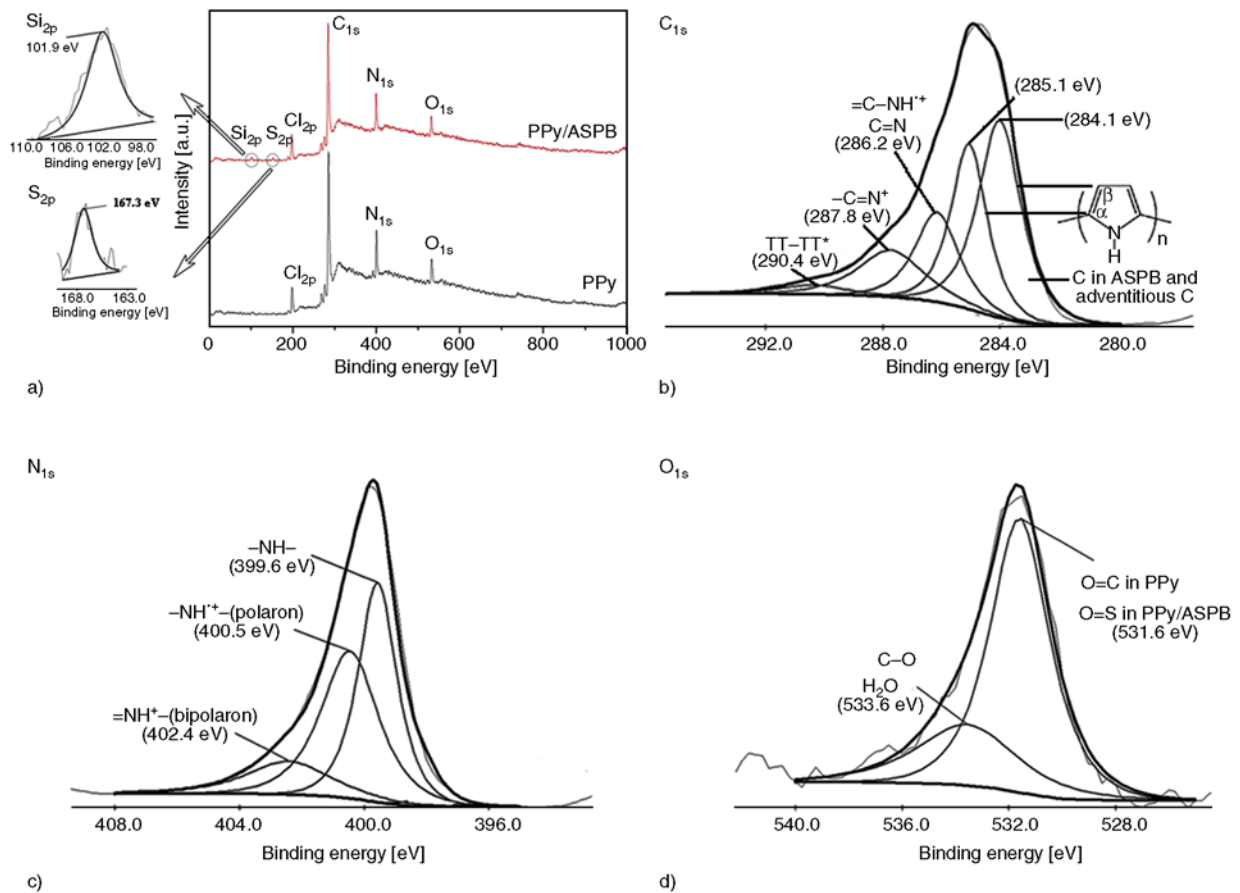

Figure 6. XPS spectra of (a) wide region spectroscopy, (b) C_{1s}, (c) N_{1s}, (d) O1s of PPy/ASPB nanocomposite

tered peak at 285.1 eV corresponds to α- carbons. Three other peaks are identified by the deconvolution of the signal at 286.2, 287.8 and 290.4 eV, respectively belonging to the defects in doped PPy. According to the literature by Ruangchuay *et al.* [29], the peak at 286.2 eV is contributed by the imine-like (C=N), polaron (=C–NH•+), hydroxylated defects (C–OH) and C–S from the dopant. The peak positioned at 287.8 eV is associated to the bipolarons (–C=N+) and carbonylic defects (C=O). The highest binding energy peak at 290.4 eV can be assigned to π-π* satellite commonly found in aromatic PPy, 6.3 eV higher than that of the main C peak.

As shown in Figure 6c, the deconvolution of N_{1s} signals in the XPS spectrum gives three Gaussian components. The main N peak at 399.6 eV is attributed to the neutral N in the Py ring (–NH–). The imine-like nitrogen (=N–) is disappeared while two new peaks at high binding energy are present [30]. The high binding energy peak can be attributed to oxidized/protonated N. Comparing to the position of the main peak, the 0.9 eV higher binding energy (400.5 eV) peak is indicative of –NH•+– in the polaron charge carrier species, while the 2.8 eV higher binding energy (402.4 eV) peak can be assigned to =NH+–, a bipolaron charge carrier species [31]. Upon consideration of the literature, the nitrogen signal of dedoped PPy only has three peaks at about 397.8, 399.7, and 400.5 eV. The present set of peaks is shifted to higher binding energy compared to that of PPy.

The oxygen signal (O_{1s}) in the XPS spectrum is shown in Figure 6d. Two peaks at 531.6 and 533.6 eV are found from the deconvolution of the signal. The peak at 531.6 eV can be attributed to the O=S of the dopant present in the PPy/ASPB nanocomposite [32], while the peak located at 533.6 eV may be related to the oxygen contribution of bound water and polymer-oxidized moieties.

XPS studies indicate that doping of ASPB into PPy matrix is achieved, as expected, which is consistent with both FTIR studies.

3.5. Measurements of electrical conductivity

The electrical conductivities of PPy and PPy/ASPB nanocomposite are determined using a RTS-4 four point probe resistivity measurement system. Results indicate that the room temperature electrical conductivity of PPy is 3.6 S/cm, however, PPy/ASPB nanocomposite shows a high value of conductivity (20 S/cm). Also, it is higher than those reported by literatures, including PPy-grafted multiwalled carbon nanotube (MWCNT) [25], polypropylene (PP)/montmorillonite (MMT)/PPy nanocomposites [33], PPy/SiO$_2$ nanocomposite [34] and PPy/PSS core-shell nanoparticles [35]. Increase in magnitude of conductivity is consistent with the FTIR and Raman spectra results.

3.6. Thermal gravimetric analysis

Figure 7 displays the thermal gravimetric analysis of PPy, ASPB and PPy/ASPB nanocomposite under N_2 and O_2 atmospheres at 60% RH. As observed from the Figure 7a, it demonstrates that the thermal stability of ASPB is much higher than that of PPy in the temperature range of 35–750°C. As PPy is hygroscopic, nearly 7.9 wt% weight loss has occurred at 100°C, due to the evaporation of residual water while only 2 wt% weight loss for PPy/ASPB nanocomposite. As the temperature increases, the main mass loss of PPy and PPy/ASPB nanocomposite starts at about 250°C corresponding to PPy degradation [36]. In case of PPy, the weight reduces largely with only one endothermic peak at 286°C observed in Figure 7b. However, a considerable enhancement in thermal stability has been seen for PPy/ASPB nanocomposite. Finally at 600°C, weight loss for PPy is almost 100%, much more than that for PPy/ASPB nanocomposite (25%). The increase of PPy/ASPB nanocomposite residual content can also be displayed in Figure 7c. Compared with the DSC curve of PPy at N_2 atmosphere (Figure 7b), the curve of PPy under O_2 atmosphere (Figure 7d) shows the end of a sharp exothermic peak at 475.5°C because of additional oxygen involving in the reaction [37]. For the DSC curve of PPy/ASPB nanocomposite, the exothermic peaks are not obvious and move to the high temperature. All the results show that introducing ASPB into the PPy system can enhance the thermal stability of PPy. The improvement in the thermal stability can also be attributed to the increase in orderliness of PPy chains, supported by analysis of XRD, SEM and conductivity measurements.
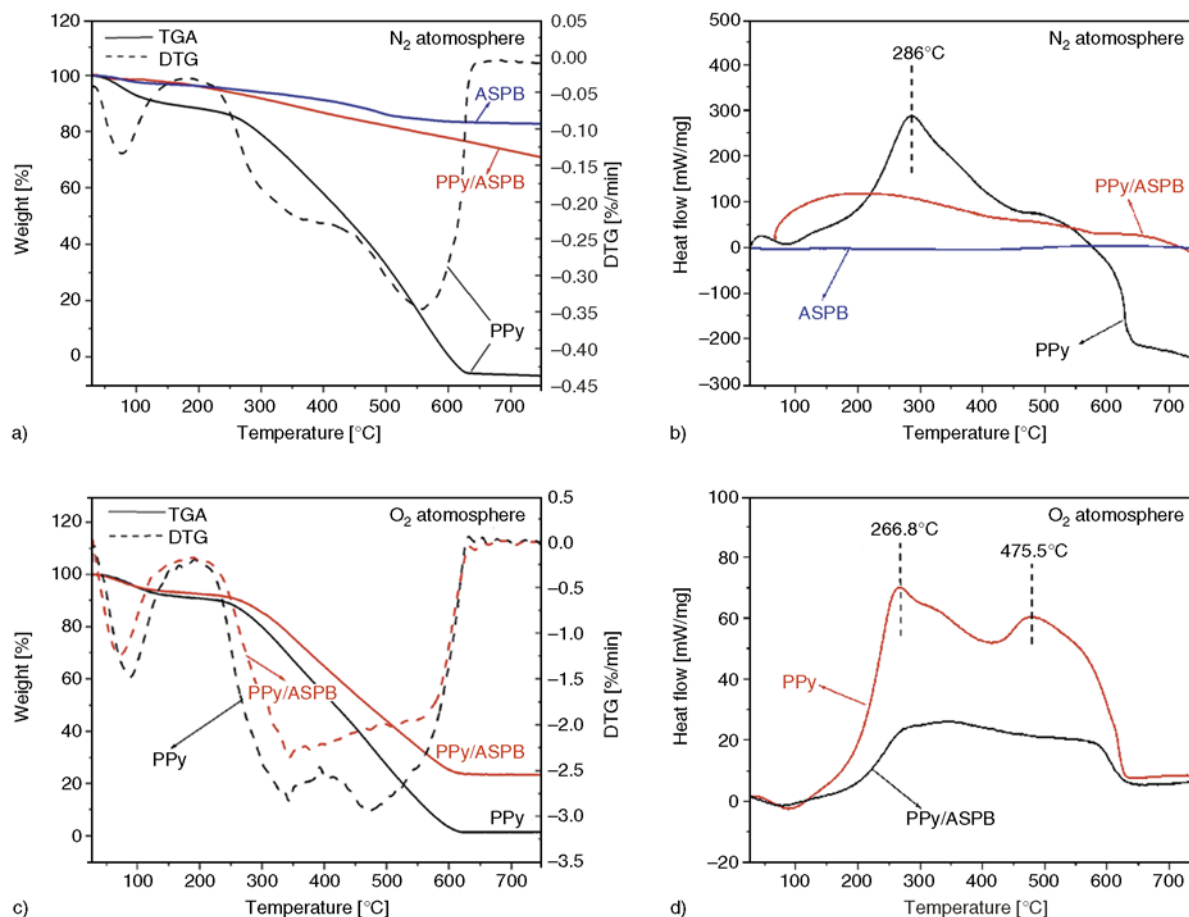
Figure 7. Thermal gravimetric analysis of PPy, ASPB and PPy/ASPB nanocomposite under N_2 atmosphere (a, b) and under O_2 atmosphere (c, d)

4. Conclusions

In summary, novel PPy/ASPB nanocomposite by means of *in situ* chemical oxidation polymerization method has been described. Different characterization and analytical methods confirm that ASPB is an excellent dopant for PPy. Compared with PPy, PPy/ASPB nanocomposite possesses the appearance of sphere-like morphology, enhanced thermal stability and higher room temperature electrical conductivity. Therefore, for the doped PPy system, more work is certainly necessary to validate the above treatment for other intrinsically conducting polymers.

Acknowledgements

References

[1] Shirakawa H., Louis E. J., MacDiarmid A. G., Chiang C. K., Heeger A. J.: Synthesis of electrically conducting organic polymers: Halogen derivatives of polyacetylene, $(CH)_x$. Journal of the Chemical Society, Chemical Communications, **16**, 578–580 (1977).
DOI: 10.1039/C39770000578

[2] Jang J., Nam Y., Yoon H.: Fabrication of polypyrrole–poly(N-vinylcarbazole) core–shell nanoparticles with excellent electrical and optical properties. Advanced Materials, **17**, 1382–1386 (2005).
DOI: 10.1002/adma.200401841

[3] Wu T-M., Lin S-H.: Synthesis, characterization, and electrical properties of polypyrrole/multiwalled carbon nanotube composites. Journal of Polymer Science Part A: Polymer Chemistry, **44**, 6449–6457 (2006).
DOI: 10.1002/pola.21724

[4] Carrasco P. M., Grande H. J., Cortazar M., Alberdi J. M., Areizaga J., Pomposo J. A.: Structure–conductivity relationships in chemical polypyrroles of low, medium and high conductivity. Synthetic Metals, **156**, 420–425 (2006).
DOI: 10.1016/j.synthmet.2006.01.005

[5] DeArmitt C., Armes S. P.: Colloidal dispersions of surfactant-stabilized polypyrrole particles. Langmuir, **9**, 652–654 (1993).
DOI: 10.1021/la00027a007

[6] Yuan X., Zeng X., Zhang H-J., Ma Z-F., Wang C-Y.: Improved performance of proton exchange membrane fuel cells with *p*-toluenesulfonic acid-doped Co-PPy/C as cathode electrocatalyst. Journal of the American Chemical Society, **132**, 1754–1755 (2010).
DOI: 10.1021/ja909537g

[7] Lee J. Y., Kim D. Y., Kim C. Y.: Synthesis of soluble polypyrrole of the doped state in organic solvents. Synthetic Metals, **74**, 103–106 (1995).
DOI: 10.1016/0379-6779(95)03359-9

[8] Lee J. Y., Song K. T., Kim S. Y., Kim Y. C., Kim D. Y., Kim C. Y.: Synthesis and characterization of soluble polypyrrole. Synthetic Metals, **84**, 137–140 (1997).
DOI: 10.1016/S0379-6779(97)80683-2

[9] Oh E. J., Jang K. S., Suh J. S., Kim H., Kim K. H., Yo C. H., Joo J.: UV-Vis./NIR and transport studies of chemically synthesized soluble polypyrrole. Synthetic Metals, **84**, 147–148 (1997).
DOI: 10.1016/S0379-6779(97)80686-8

[10] Shen Y., Wan M.: In situ doping polymerization of pyrrole with sulfonic acid as a dopant. Synthetic Metals, **96**, 127–132 (1998).
DOI: 10.1016/S0379-6779(98)00076-9

[11] Wu T-M., Chang H-L., Lin Y-W.: Synthesis and characterization of conductive polypyrrole with improved conductivity and processability. Polymer International, **58**, 1065–1070 (2009).
DOI: 10.1002/pi.2634

[12] Cairns D. B., Armes S. P., Chehimi M. M., Perruchot C., Delamar M.: X-ray photoelectron spectroscopy characterization of submicrometer-sized polypyrrole–polystyrene composites. Langmuir, **15**, 8059–8066 (1999).
DOI: 10.1021/la990443k

[13] Jaramillo A., Spurlock L. D., Young V., Brajter-Toth A.: XPS characterization of nanosized overoxidized polypyrrole films on graphite electrodes. Analyst, **124**, 1215–1221 (1999).
DOI: 10.1039/A902578B

[14] Ruangchuay L., Schwank J., Sirivat A.: Surface degradation of α-naphthalene sulfonate-doped polypyrrole during XPS characterization. Applied Surface Science, **199**, 128–137 (2002).
DOI: 10.1016/S0169-4332(02)00564-0

[15] Nicho M. E., Hu H.: Fourier transform infrared spectroscopy studies of polypyrrole composite coatings. Solar Energy Materials and Solar Cells, **63**, 423–435 (2000).
DOI: 10.1016/S0927-0248(00)00061-1

[16] Ekramul Mahmud H. N. M., Kassim A., Zainal Z., Yunus W. M. M.: Fourier transform infrared study of polypyrrole–poly(vinyl alcohol) conducting polymer composite films: Evidence of film formation and characterization. Journal of Applied Polymer Science, **100**, 4107–4113 (2006).
DOI: 10.1002/app.23327

[17] Menon V. P., Lei J., Martin C. R.: Investigation of molecular and supermolecular structure in template-synthesized polypyrrole tubules and fibrils. Chemistry of Materials, **8**, 2382–3290 (1996).
DOI: 10.1021/cm960203f

[18] Baughman R. H., Shacklelette L. W.: Conductivity as a function of conjugation length: Theory and experiment for conducting polymer complexes. Physical Review B, **39**, 5872–5886 (1989).
DOI: 10.1103/PhysRevB.39.5872

[19] Pruneanu S., Graupner W., Oniciu L., Brie M., Turcu R.: Electrochemical and X-ray diffraction studies on polypyrrole films. Materials Chemistry and Physics, **46**, 55–60 (1996).
DOI: 10.1016/0254-0584(96)80130-1

[20] Ormond-Prout J., Dupin D., Armes S. P., Foster N. J., Burchell M. J.: Synthesis and characterization of polypyrrole-coated poly(methyl methacrylate) latex particles. Journal of Materials Chemistry, **19**, 1433–1442 (2009).
DOI: 10.1039/b816839c

[21] Gu Z., Zhang L., Li C.: Preparation of highly conductive polypyrrole/graphite oxide composites via *in situ* polymerization. Journal of Macromolecular Science Part B: Physics, **48**, 1093–1102 (2009).
DOI: 10.1080/00222340903035576

[22] Gao J-W., Li G., Yao Y-F., Jang J-M.: Preparation and characterization of montmorillonite/polypyrrole nanocomposites by in-situ chemical polymerization. Journal of Macromolecular Science Part B: Physics, **50**, 1364–1375 (2011).
DOI: 10.1080/00222348.2010.497688

[23] Joo J., Lee J. K., Baeck J. S., Kim K. H., Oh E. J., Epstein J.: Electrical, magnetic, and structural properties of chemically and electrochemically synthesized polypyrroles. Synthetic Metals, **117**, 45–51 (2001).
DOI: 10.1016/S0379-6779(00)00537-3

[24] Shen Y., Wan M.: Soluble conductive polypyrrole synthesized by *in situ* doping with β-naphthalene sulphonic acid. Journal of Polymer Science Part A: Polymer Chemistry, **35**, 3689–3695 (1997)
DOI: 10.1002/(SICI)1099-0518(199712)35:17<3689:: AID-POLA8>3.0.CO;2-N

[25] Jeon I-Y., Choi H-J., Tan L-S., Baek J-B.: Nanocomposite prepared from *in situ* grafting of polypyrrole to aminobenzoyl-functionalized multiwalled carbon nanotube and its electrochemical properties. Journal of Polymer Science Part A: Polymer Chemistry, **49**, 2529–2537 (2011).
DOI: 10.1002/pola.24684

[26] Demoustier-Champagne S., Stavaux P. Y.: Effect of electrolyte concentration and nature on the morphology and the electrical properties of electropolymerized polypyrrole nanotubules. Chemistry of Materials, **11**, 829–834 (1999).
DOI: 10.1021/cm9807541

[27] Gupta S.: Hydrogen bubble-assisted syntheses of polypyrrole micro/nanostructures using electrochemistry: Structural and physical property characterization. Journal of Raman Spectroscopy, **39**, 1343–1355 (2008).
DOI: 10.1002/jrs.2002

[28] Luo Y-L., Fan L-H., Xu F., Chen Y-S., Zhang C-H., Wei Q-B.: Synthesis and characterization of Fe_3O_4/PPy/P(MAA-co-AAm) trilayered composite microspheres with electric, magnetic and pH response characteristics. Materials Chemistry and Physics, **120**, 590–597 (2010).
DOI: 10.1016/j.matchemphys.2009.12.002

[29] Ruangchuay L., Schwank J., Sirivat A.: Surface degradation of α-naphthalene sulfonate-doped polypyrrole during XPS characterization. Applied Surface Science, **199**, 128–137 (2002).
DOI: 10.1016/S0169-4332(02)00564-0

[30] MacDiarmid A. G., Epstein A. J.: Polyanilines: A novel class of conducting polymers. Faraday Discussions of the Chemical Society, **88**, 317–332 (1989).
DOI: 10.1039/DC9898800317

[31] Malitesta C., Losito I., Sabbatini L., Zambonin P. G.: New findings on polypyrrole chemical structure by XPS coupled to chemical derivatization labelling. Journal of Electron Spectroscopy and Related Phenomena, **76**, 629–634 (1995).
DOI: 10.1016/0368-2048(95)02438-7

[32] Andreoli E., Rooney D. A., Redington W., Gunning R., Breslin C. B.: Electrochemical deposition of hierarchical micro/nanostructures of copper hydroxysulfates on polypyrrole–polystyrene sulfonate films. The Journal of Physical Chemistry C, **115**, 8725–8734 (2011).
DOI: 10.1021/jp200465n

[33] Omastová M., Mravčaková M., Chodák I., Pionteck J., Häussler L.: Conductive polypropylene/clay/polypyrrole nanocomposites. Polymer Engineering and Science, **46**, 1069–1078 (2006).
DOI: 10.1002/pen.20551

[34] Yuvaraj H., Shim J-J., Lim K. T.: Organic–inorganic polypyrrole-surface modified SiO_2 hybrid nanocomposites: A facile and green synthetic approach. Polymers for Advanced Technologies, **21**, 424–429 (2010).
DOI: 10.1002/pat.1448

[35] Mpoukouvalas K., Wang J., Wegner G.: Conductivity of poly(pyrrole)-poly(styrene sulfonate) core–shell nanoparticles. ChemPhysChem, **11**, 139–148 (2010).
DOI: 10.1002/cphc.200900643

[36] Bose S., Kuila T., Uddin M. E., Kim N. H., Lau A. K. T., Lee J. H.: In-situ synthesis and characterization of electrically conductive polypyrrole/graphene nanocomposites. Polymer, **51**, 5921–5928 (2010).
DOI: 10.1016/j.polymer.2010.10.014

[37] Beck F., Braun P., Oberst M.: Organic electrochemistry in the solid state-overoxidation of polypyrrole. Berichte der Bunsen-Gesellschaft, **91**, 967–974 (1987).